Microstructure Profiling with the High Resolution Profiler

Kurt L. Polzin and Ellyn T. Montgomery

Woods Hole Oceanographic Institution

Woods Hole, Massachusetts 02543-1541

Abstract

The High Resolution Profiler (HRP) is a unique oceanographic instrument used to collect fine- and microstructure data at sea. During it's ten years of use in experiments the methods of analyzing the microstructure data from the HRP have been evolving. The purpose of this report is to summarize the processing of the microstructure data collected by the HRP and document the instrument's noise levels.

1 Introduction

The HRP is an oceanic free fall vehicle designed at the Woods Hole Oceanographic Institution to collect fine- and microstructure data as it descends through the water column. The term "microstructure" is used to refer to processes occurring on scales smaller than 1/2 meter in the vertical. Finescale and finestructure imply larger length scales. Different suites of sensors are employed by the HRP to sense velocity, temperature and conductivity variability over these different regimes. This report documents the micro-scale processing and noise levels of the HRP, and serves as a companion paper to the report of Schmitt, *et al.* (1988), which documents the profiler, its development, and the finescale sensors.

The primary goal of the microstructure processing is the accurate estimation of gradient variances (e.g. $< T_z^2 >$) in the water column. Much of the computational effort supports the central issues of signal to noise optimization, calibrations and corrections for electronic and sensor transfer functions. The microstructure processing algorithms are based upon those developed by N. Oakey (personal communication, 1990). The result of combining the HRP instrumentation and processing algorithms is lower noise levels than those quoted for other microstructure platforms.

This report is organized into sections as described below: a short summary of the HRP and its use in collecting fine- and microstructure data is be presented in section 2; in section 3 we discuss an interpretation of the microstructure data to motivate consideration of the processing; a description of the microstructure sensors used on the HRP and corrections for the sensor response transfer functions is presented in section 4; section 5 documents the processing steps, the microstructure noise levels are quantified in section 6; and the summary is given in section 7.

2 High Resolution Profiler Description

The High Resolution Profiler (HRP) is a vertically profiling free vehicle (ie. it is an instrument that is not attached to the ship that collects data as it falls vertically through the water column). Being a free vehicle, the measurements taken by the HRP are not subject to cable induced noise. Each deployment of the HRP, and the data collected during that deployment, is referred to as a station or profile. The instrument is 5 meters long and has a diameter of a half meter.

The HRP was designed and developed at WHOI to make high quality fine- and microstructure measurements using the interface bus computer [IBC, Mellinger *et al.* (1986)]. The IBC is the HRP's controller; handling everything from software setup to data acquisition and storage. A suite of sensors interfaced to the IBC provide data describing the physical properties of the water sampled as the HRP descends. All the data collected is stored internally in a 16 Mb RAM (random access memory) mass storage area. A schematic of the HRP and its components is shown in Figure 1. For additional information on the development of the HRP and IBC, see the papers by Schmitt *et al.* (1988) and Mellinger *et al.* (1986).

The HRP has two data streams: "fine" and "micro". The data acquisition for each stream is commenced when the measured pressure exceeds a user defined threshold. Data acquisition (and the dive) is terminated when the first of pressure, acoustic range or time criteria is reached. The fine-scale data consists of inputs from the on-board CTD (conductivity, temperature, depth sensor), and a suite of analog devices are interfaced with the analog to digital (A/D) converter channels. During a profile, microstructure measurements of turbulent velocity, as well as temperature and conductivity fluctuations are acquired simultaneously with the finescale data. The sampling in both modes is driven by the 200 Hz interrupt, with microscale data acquired every cycle, and finescale data acquired every twentieth cycle, for a rate of 10 Hz.

The nominal fall rate of the HRP is 0.65 meters/sec. With the given sampling rates, fine data is collected nominally every 0.065 meters and microstructure data is collected every 0.0033 meters. The fine-scale data is bin averaged over 0.5 db intervals. Estimates of microstructure variances are centered about the 0.5 db bins.

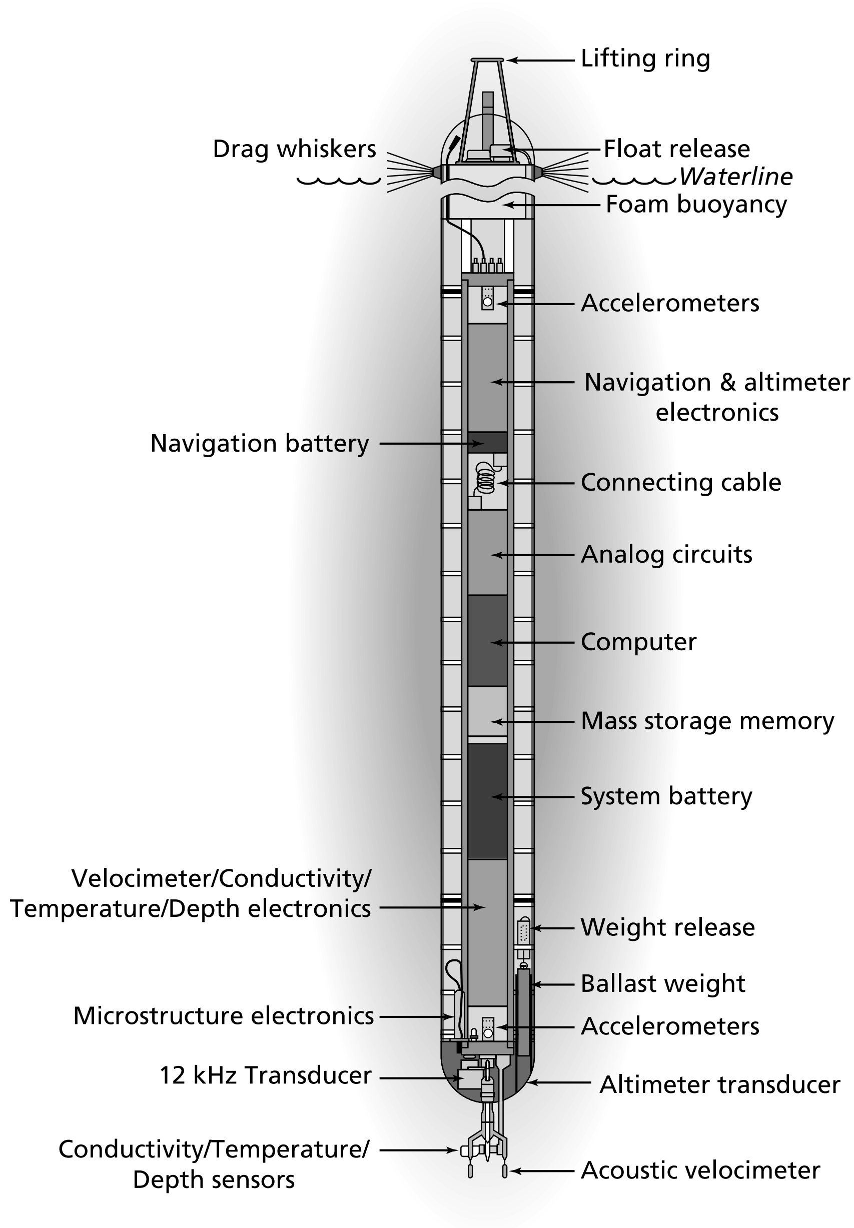

Figure 1: Schematic of the High Resolution Profiler (HRP)

The HRP has been used on five major scientific cruises after its debut during the FASINEX program. In order to provide background chronology and relate the processing to the instrument's use, the following paragraphs summarize the use of the HRP in experiments at sea. More detailed information about these experimental programs is available in Schmitt and Montgomery (1991); Montgomery and Toole (1993); Montgomery and Schmitt (1993); Montgomery (1996) and Montgomery (unpublished).

- FASINEX - Frontal Air-Sea Interaction Experiment: February, 1986 near Bermuda. Completed 39 dives, the deepest of which reached 1000 meters.
- WRINCLE - Warm Ring Inertial Critical Layer Experiment: March, 1990 in the Western North Atlantic. Completed 78 dives to 1000 meters in and around a Gulf Stream warm core Ring.
- TOPO - Mixing near Abrupt Topography Experiment: April, 1991 in the Eastern Subtropical Pacific at Feiberling Guyot. Completed 108 dives of 500 - 3000 meters above and around the seamount as part of the Abrupt Topography Accelerated Research Initiative.
- NATRE - North Atlantic Tracer Release Experiment: April, 1992 in the Canary Basin of the Eastern North Atlantic. Completed 155 dives of 2000 - 4000 meters while surveying the area targeted for the tracer release.
- ROMEL - ROmanche MELange: November, 1994 in the vicinity of the Romanche and Chain Fracture Zones in the Eastern Equatorial Atlantic. Completed 53 dives, 45 to full ocean depth. The deepest dive was to 5202 meters.
- BBTRE1 - Brazil Basin Tracer Release Experiment - year 1: Completed 75 dives, 74 to full ocean depth while surveying the basin and regions targeted for tracer release. Most of these profiles went to between 4000 and 5000 meters, the deepest dive was to 5651 meters.

3 Interpretation of Microstructure Data

The Cox-Osborn relation (Osborn and Cox, 1972) and Osborn's (1980) method interpret the rate of dissipation of turbulent kinetic energy and rate of dissipation of thermal variance in terms of stationary, homogeneous, isotropic turbulence resulting from production-dissipation balances, with 'background' gradients only in the vertical:

$$< u'w' >< du/dz >= -\frac{g}{\rho} < w'\rho' > -\epsilon$$

(Turbulent Kinetic Energy Equation)

$$2 < w'T' >< dT/dz + \Gamma >= -\chi$$

(Turbulent Heat Equation),

where ϵ is the rate of dissipation of turbulent kinetic energy, χ is the rate of dissipation of thermal variance and Γ is the adiabatic lapse rate. The flux Richardson number, R_f, is defined as the ratio between the buoyancy and momentum fluxes:

$$R_f = -\frac{g}{\rho} < w'\rho' > / < u'w' >< du/dz > .$$

The flux Richardson number is generally assumed to be constant within the oceanographic context [see Holt *et al.* (1992) for an insightful discussion]. Values of $R_f = 0.15$ (Osborn, 1980) or $R_f = 0.2$ (Oakey,

1982) are generally assumed. Given a constant flux Richardson number, the turbulent kinetic energy equation can be written as (Osborn, 1980):

$$\frac{g}{\rho} < w'\rho' >= \frac{R_f}{1-R_f}\epsilon \quad .$$

Diffusivities result from parameterizing the buoyancy flux and the temperature flux as a constant times a gradient, i.e. the usual eddy coefficient formulation:

$$\begin{aligned} K_\rho &= \frac{R_f}{1-R_f}\frac{\epsilon}{N^2} \\ K_T &= \frac{\chi}{2 < \theta_z >^2} \end{aligned} \tag{1}$$

Estimates of the rate of dissipation of turbulent kinetic energy, ϵ, are created by averaging the two components of shear variance and assuming isotropy (Itsweire *et al.*, 1993). Estimates of the rate of dissipation of thermal variance, χ, are produced also assuming isotropy:

$$\epsilon = 3.75\nu \left[< u_z'^2 > + < v_z'^2 > \right] \ ,$$

$$\chi = 6\kappa < T_z^2 > \quad ,$$

with ν and κ the molecular viscosity and thermal diffusivity, respectively.

Given this approach, the problem of estimating the eddy diffusivity is reduced to one of estimating the turbulent temperature and velocity gradient variances as accurately as possible. The determination of thermistor time constants, microtemperature and conductivity calibrations and processing methods described below are dedicated to this end.

4 Description of Microstructure Sensors used on the HRP

The HRP records four microstructure quantities: two axes of shear, temperature and conductivity gradients. They are sensed with airfoil probes (Osborn, 1974; Osborn and Crawford, 1980), an FP07 fast response thermistor (Gregg *et al.*, 1986), and a dual electrode conductivity cell (Meagher *et al.*, 1982), respectively. In FASINEX, shear probes designed by Dr. N. Oakey (Bedford Institute of Oceanography) were used. In later experiments, probes constructed by Mr. E. Schiemer to a design of Dr. R. Lueck (Univ. of Victoria) were employed. Both the temperature and conductivity microstructure sensor assemblies were purchased from Sea-Bird Electronics, Inc. Estimates of χ are made with both the microtemperature and microconductivity sensors. The two estimates are distinguished below by the subscripts θ and C. Shear probe electronics were constructed to a design of Dr. N. Oakey. The text below describes the electronic transfer functions, corrections for sensor response and calibration procedures.

The microstructure data were electronically premphasized in the HRP prior to digitization to reduce quantization errors. The temperature and conductivity transfer functions are white at low frequencies, resemble first-difference operators (i.e. ω^2 between .1 and 200 Hz), and are white at higher frequencies. The data from the air-foil velocity probes are premphasized with a filter which resembles a first-difference operator until 100 Hz, whereupon it falls as ω^{-2}. Four-pole Butterworth filters with half-power points at 100 Hz are additionally applied to all microstructure channels as anti-aliasing filters (50 Hz for field programs following TOPO).

The airfoil velocity probe spatially averages the three dimensional turbulent velocity field in a complicated manner which depends on the turbulent energy spectrum (Ninnis, 1984). A single-pole transfer function with a half-power point at 2 cm was used to correct the shear spectra from the FASINEX experiment. This approach was taken so that the HRP and EPSONDE (Oakey, 1977) data would be consistent in this respect. The algebraic correction of Ninnis (1984), was used to correct later shear data obtained with the sensors designed by R. Lueck.

The response time of the thermistor is limited by the time for temperature fluctuations to diffuse through the glass coating and fluid boundary layer (which is related to the rate of descent) surrounding the sensor. The spectral response of microbead thermistors has been well documented [Lueck *et al.*, 1977; Gregg *et al.*, 1978; Lueck and Osborn, 1980; Gregg and Meagher, 1980]. Lueck *et al.* (1977) originally suggested that the transfer function should be aptly described by a single-pole transfer function for small frequencies and that no asymptotic high frequency functional form was apparent from their analytical results. Gregg *et al.* (1978), in a later work, found that the high frequency dynamic response of such thermistors was sufficiently well described by a double-pole transfer function. For fall speeds of .6 m/s, there appears to be little difference in Gregg *et al.* (1978)'s fitted single and double-pole transfer functions as long as the gain correction does not exceed an order of magnitude.

The HRP FP07 thermistor data was corrected assuming a single-pole transfer function. The time constant was determined from fits to the ratio between the microconductivity and microtemperature spectra for regions of large density ratio (R_ρ) and large thermal dissipation rate (χ). The criterion of large R_ρ ensures that the salinity spectrum has a small contribution to the conductivity spectrum. The criterion of large χ ensures the transfer function will not be affected by either sensor's noise spectrum. The analysis was repeated for each individual thermistor used. The single-pole form was employed as it appeared to give a better representation of the microtemperature-microconductivity transfer function at low frequencies for the HRP data.

The time constant was estimated as follows. Individual 0.5 db micro-temperature and conductivity gradient spectra are reviewed to select those having large signal to noise ratios to at least 50 Hz. A high resolution density ratio profile was then plotted to confirm that the selected data coincides with a region of large density ratio (minimally $R_\rho > 5$). Average micro-temperature and conductivity gradient spectra are generated by normalizing individual spectra by their respective variances. A minimum of 25 and preferably 50 to 100 0.5 db data segments are required to estimate the temperature-conductivity transfer function from the average spectra. A linear least-squares fit between the inverse of the observed transfer function and that corresponding to a single pole filter, $y = a + b\omega^2$, is then performed to estimate the thermistor time constant, $1/(\omega_c) = (a/b)^{1/2}$. Finally, the time constant is corrected for fall rate dependence of the fluid boundary layer height as $\tau = (w/w_{ref})^{0.32}/2\pi\omega_c$, with w the profiler descent rate determined from the pressure record $(w \sim dp/dt)$ and w_{ref} the descent rate for the pressure interval from which the transfer function was determined.

The microconductivity cell was not corrected for any effects of spatial averaging. The dual needle cell had a centerline to centerline separation of 3mm. The electrical field of such a sensor is approximately a dipole with 95% of the field within two centerline separations (Head, 1983). Given a sampling rate of 200 Hz and a fall speed of .65 m/s, the Nyquist wavenumber, 1/6mm, is roughly equal to the averaging interval. Meagher *et al.* (1982); Okawa and Dugan (1984) and Dugan and Stalcup (1988), have established that the half-power point of the conductivity probe is approximately 100 cpm. Frequencies of less than 50 Hz were therefore relatively unaffected by any effects of averaging by the needle cell.

The calibrations for the micro-data are derived from a number of sources. Laboratory calibrations provided by R. Lueck (WRINCLE) and with the assistance of Dr. N. Oakey (other field programs) were applied to the shear probes. The microtemperature and microconductivity data are calibrated with local regressions against the in situ CTD data. In order to accomplish this, the effects of the premphasis filter were removed with a recursive digital filter described in Schmitt *et al.* (1988) to create temperature and conductivity profiles. Prior to deconvolving the micro-profiles, those data were despiked with a first difference operator. The micro-profiles were then regressed to the 0.5 db CTD data in fits of 21 points. A two-hundred point running mean of the microtemperature and microconductivity calibrations was then taken, and points that deviated from the running mean by greater than 10% were replaced by the mean. The calibrations were then smoothed twice with a 51 point box-car filter. Vertical profiles of microtemperature and microconductivity calibrations are repeatable to within $\pm 5\%$ in regions having non-zero gradients over large vertical scales (e.g. outside the mixed layer).

With some experience in the selection of spectra, the time constant calculation is repeatable to 10%. We have attempted to asses the impact of a 10% error in the time constant upon the thermal eddy diffusivity estimate in the following manner. The true temperature spectrum was assumed to be represented by the Batchelor spectrum. The variance represented by that spectrum for given $(\epsilon,\ \chi_\theta,\ N,\ K_T)$ was calculated. The Batchelor spectrum was then multiplied by

$$[1+(\frac{\omega}{\omega_c})^2]\ [1+(\frac{\omega}{1.1\omega_c})^2]$$

with

$$\omega_c = 20Hz$$

and the variance recalculated. The ratio between the two determines how error in the time constant propagates through to the estimation of the eddy diffusivity. Error estimates are tabulated below in Table 1 for two values of the background stratification rate assuming no salinity gradient. The error in K_T associated with a 10% uncertainty in the time constant is generally less than 10% unless the dissipation rate (ϵ) is large.

Table 1

Estimates of the propagation error in K_T associated with 10% uncertainties in the thermistor time constant. In A, p =3000 db and $T = 4$°C. In B, $p = 1000$ db and $T = 13$°C. K_T is the turbulent thermal diffusivity $(x10^{-4}$ m^2 s^{-1}), N the buoyancy frequency (s^{-1}), ϵ the dissipation rate of turbulent kinetic energy (W/kg), χ_θ the rate of thermal dissipation (°C^2 s^{-1}) and the percent error in the estimate of χ_θ induced by a 10% error in the determination of the thermistor time constant. The profiler fall rate was assumed to be 0.6 m/s.

	K_T	N	ϵ	χ_θ	err %
	0.1	.00524	1.1E-9	3.9E-9	7
A	1.0	.00524	1.1E-8	3.9E-8	11
	10.0	.00524	1.1E-7	3.9E-7	15
	0.1	.001	4.0E-11	9.0E-12	2
B	1.0	.001	4.0E-10	9.0E-11	4
	10.0	.001	4.0E-9	9.0E-10	8

5 Microstructure Processing Algorithms

The goal of the analysis of microstructure data from the HRP is to produce an accurate spectrum of oceanic shear, microtemperature or microconductivity from which to compute the variance. The process of treating the data can be delineated into the following steps: scaling, application of spectral corrections, signal to noise optimization and quality control procedures. The scaling and sensor related corrections are described above. This section seeks to address the remainder, which can be characterized as more software oriented.

The premphasized microstructure data were analyzed as segments of 256 or 512 points centered on the 1/2 db bin-averaged finestructure data. The microstructure data were read in, a two-pole, 10 Hz Butterworth recursive filter applied to the shear probe data to reduce the amplitude of a vibrational spike at 30-40 Hz (Figure 2) and then aligned with the finescale data. The calibrations were then applied to the individual data points. After calculating the fall rate from the pressure record, the data was transformed from a time series to a spatial series by invoking Taylor's hypothesis.

The next step in processing is to check for the presence of spikes. The 256 (512) points are divided into 10 intervals and variances calculated for each of interval. The variances were ordered by magnitude and the smallest nine averaged. If the average variance exceeded α times the average of the nine smallest, that variable and segment of 256 (512) points was flagged as being potentially noisy. A similar scheme was discussed by Marmarino *et al.* (1986). Such spikes are due to a number of causes: a 10 kHz transponder used for tracking the profiler, plankton impacts and fouling of the microconductivity and microtemperature sensors by detritus. The particular value of α employed is dependent upon signal levels, sensor type and the use of the recursive filter for the shear data. Appropriate values of α can be selected by plotting the average variance vs the average of nine intervals having the smallest variance and choosing α to cull the outlying several percent of the data. Typical values for α are 1.5$-$2 (shear) and 2.5$-$3 (conductivity/temperature).

The 256 (512) points were then detrended with a least squares fit, windowed with 50% cosine tapers (Hanning window) and then fast-Fourier transformed. The microconductivity/microtemperature cospectrum was also computed. Spectral density estimates were created by multiplying the Fourier coefficients by their complex conjugates and corrected for the loss of variance implied by the windowing procedure.

All spectral corrections are then applied to the spectral density estimates. The corrections come in three basic flavors. The first is for the recursive filter applied to the shear probe data. The spectral characteristics of the applied filter can be computed exactly and the correction is straightforward. The second set corrects for the electronic premphasis and anti-aliasing filters. The theoretical and measured electronic premphasis and anti-aliasing filters agree to within $\pm$5%. The third variety of spectral corrections represent the transfer functions of the micro-sensors.

The signal to noise optimization procedures are employed in the following manner. A nine point box-car filter is applied to the spectral density estimates for individual 1/2 db spectra and a spectral minimum defined on the basis of the averaged spectra. The minimum was defined as the absolute minimum over a predetermined bandwidth. For the micro- temperature and conductivity data, the upper and lower frequencies for this calculation are 80 (80) and 20 (33) Hz, respectively. If the variance does not exceed a value corresponding to a thermal dissipation rate of $1.0x10^{-9}$ °C^2 s^{-1}, the lower bound is changed to 10 (temperature) or 20 Hz (conductivity). The use of different lower bounds for the micro-temperature and conductivity data is related to the differing shapes of the noise spectrum for the two sensors (Figure 2). For the shear probe data the upper and lower bounds are 40 and 6.25 Hz, respectively. The gradient variances are then calculated by integrating the unaveraged spectra out to the spectral minimum. If the vertical shear variance for one component is determined to be less than a corresponding dissipation rate of $5.0x10^{-10}$ W/kg, the upper bound for the spectral minimum calculation is lowered to 9.4 Hz and the lower bound set to 4.7 Hz. This is done to eliminate a secondary noise peak at 10 Hz in the shear spectra (Figure 2).

After calculating the variances, the ratio between the shear components and that between the microtemperature and conductivity is computed. If the shear data are isotropic and homogeneous over the scale of the sensor separation (10 cm), the shear components should exhibit approximately the same variances. A large disparity in variance estimates is therefore taken to indicate a potentially noisy data segment. To the degree that temperature and conductivity are redundant sensors, the gradient variances should differ by a factor of $\partial C/\partial T$, which is approximately one. This interpretation is complicated by the fact that the conductivity sensor also measures the small-scale salinity spectrum and the temperature/salinity cospectrum (e.g. Stern, 1975). If the ratio between shear components exceeded β (typically 3-5) and the ratio between temperature and conductivity exceeded γ (typically 6-10), the spectra were flagged as being potentially noisy. Selection

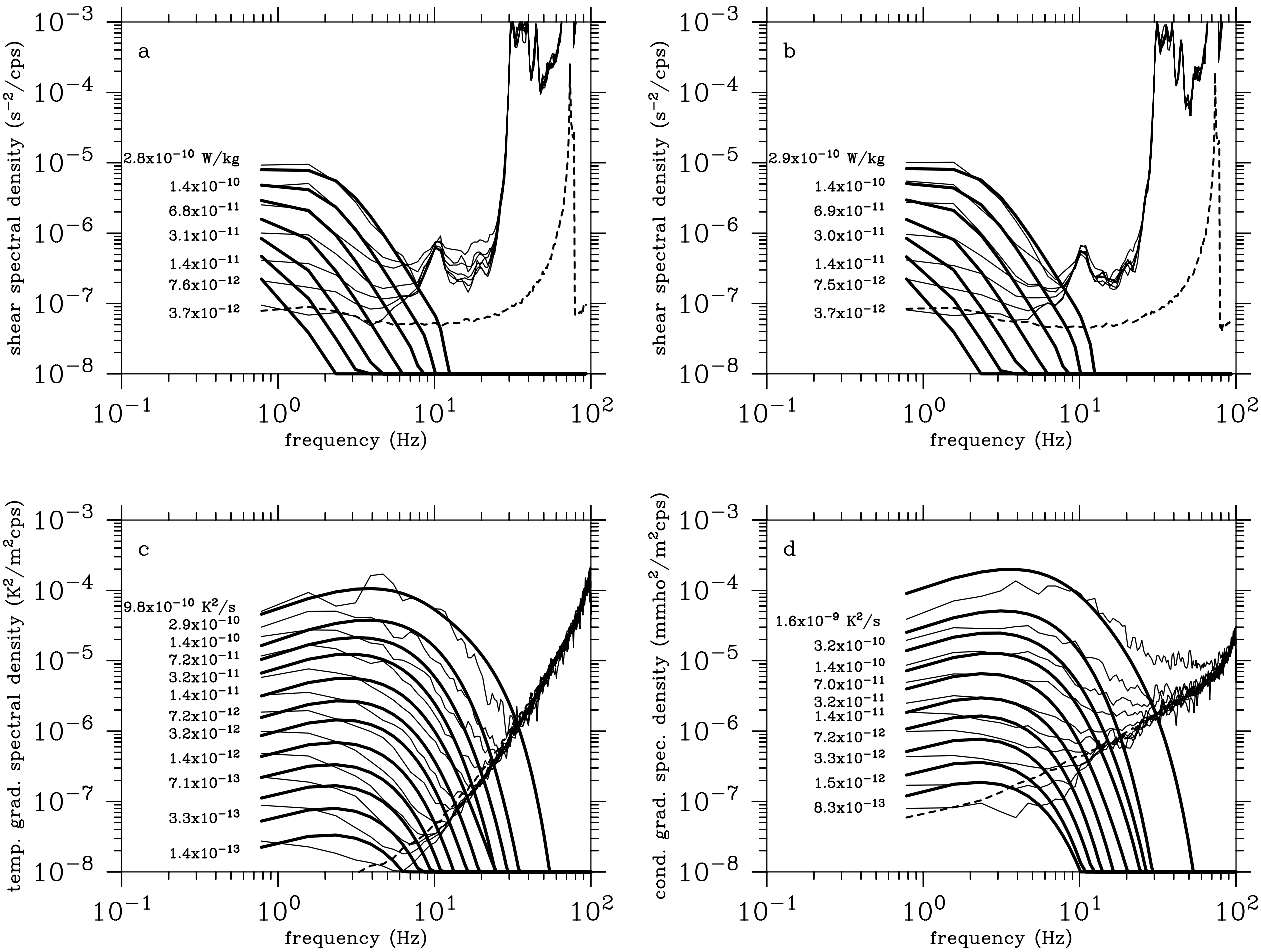

Figure 2: Microstructure spectra from 2000-3000 db for a profile in the Southeast portion of the NATRE survey grid. (a) and (b) Observed spectra for the two shear probes have been bin averaged and plotted as thin lines. Overplotted in thick lines are the bin average of the Nasmyth spectra (Oakey, 1982) for the individual spectra. Dashed lines represent the electronic noise spectra. To the left of each spectra are the bin averaged estimates of ϵ. Both the large peak at high frequencies (30-40 Hz) and the small peak at low frequency (10 Hz) in the shear spectra are believed to result from vibration. The increasing trend of both the observed and noise shear spectra at frequencies greater than 50 Hz is associated with the transfer function which accounts for the effects of the probe's spatial averaging. The transfer function is applied only for frequencies smaller than 78 Hz. A similar scheme was applied to the microtemperature (c) and microconductivity (d) gradient spectra and the Batchelor spectra (Oakey, 1982) overplotted. Relevant depth averaged parameters for these data are $N^2 = 1.1 \times 10^{-6}$ s^{-2}, $\nu = 1.52 \times 10^{-6}$ m^2 s^{-1}, $\kappa = 1.42 \times 10^{-7}$ m^2 s^{-1} and $< \theta_z >= 1.5 \times 10^{-3}$ °C m^{-1}.

of values for β and γ is somewhat subjective and depends primarily upon what patience the user has for reviewing flagged spectra.

The review of spectra which have been flagged occurs as part of the final quality control measures. In this review, spectra are regarded as noisy if they fail to reveal a spectral minimum or if substantial agreement between redundant sensors, i.e. the two shear probes and the microconductivity- microtemperature sensors, does not exist. Plots of the spectra are created for each 0.5 db data segment which has a flagged variable under the following conditions: (1) If the data segment is flagged due to a potential spike, the variance estimate has to exceed a minimum. (2) Likewise, if the spectrum is flagged because it exhibits a large variance ratio, that variance must exceed the above minimum criterion. The purpose of reviewing these spectra is to ensure that the flagged spectra are indeed noisy. In addition, a 0.5 db data segment is also plotted (but not flagged) if the variance of any variable exceeded a specified magnitude. The chosen magnitudes are intended to represent the largest several percent of the variances for a statistically homogeneous portion of the data set. Finally, depth profiles of the 0.5 db estimates of ϵ, χ_θ and χ_c are reviewed visually for the appearance of data segments which differ from neighboring data by over an order of magnitude. The spectra for such data segments are also reviewed visually.

A check on the consistency of the processing scheme and resulting variance estimates is the inferred value of the flux Richardson number, R_f (eq. 1). After averaging over the pressure range 400-800 db, the collection of HRP profiles acquired in the region of the NATRE site survey returns a value for the mixing efficiency, $< \chi_\theta >< N^2 > /2 < \epsilon >< \theta_z >^2$, of 0.24, indicating a value for R_f of 0.19. This value is consistent with those appearing in the literature [$R_f = 0.20$, Oakey (1982)] and [$R_f = 0.15$), Osborn (1980)].

6 Microstructure Sensor Noise Levels

The instrumentation and processing algorithms combine to result in lower noise levels than quoted for other microstructure platforms. The observed spectra reveal a well defined noise floor at high frequencies and remarkable agreement with universal spectral shapes at low frequencies and high dissipation rates, Figure 2. When there is good agreement between the universal curves and the observed spectra in Figure 2, the spectra are well resolved in the sense that over 90% of the variance in the universal spectra occurs at frequencies smaller than that where the universal curve intersects the noise floor (Oakey, 1982). The observed spectra substantially depart from their universal forms at low frequencies for dissipations of $2 - 3x10^{-11}$ W/kg (ϵ) and roughly $1x10^{-11}$ °C^2 s^{-1} (χ_θ). The observed conductivity gradient spectra do not agree with the Batchelor spectra, presumably because of the contribution of the salinity spectrum and temperature/salinity cospectrum to the conductivity spectrum. If interpreted as a noise estimate, a dissipation rate of $2 - 3x10^{-11}$ W/kg is a factor of two smaller than the lowest published noise levels of ϵ: $(0.5 - 1.0x10^{-10}$ W/kg; Gregg *et al.*, 1993) and roughly an order of magnitude smaller than typical noise levels of tethered platforms $(1 - 2x10^{-10}$ W/kg).

Defining noise levels on the basis of a departure of observed spectra from universal forms most likely overestimates the noise contribution. At low levels of turbulence there is little expectation that the observed spectra should retain the shapes inferred from inertial subrange arguments and found in high Reynolds number turbulence. A dissipation rate of $2 - 3x10^{-11}$ W/kg for the data displayed in Figure 2 implies an insufficient scale separation between the outer turbulent scales where buoyancy forces supress overturning [$L_o = (\epsilon N^{-3})^{1/2} \cong 0.15$ m] and those scales which are dominated by molecular viscousity,[$L_k = (\epsilon\nu^{-3})^{-1/4} \cong 0.02$ m] for the existence of an inertial subrange, invalidating the comparison between observed spectra and the universal forms (Gargett *et al.*, 1984). An alternative interpretation of the departure of observed spectra from universal forms at low signal levels is that the observed spectra represent decaying turbulence rather than noise. Seeking a more robust determination of the contribution of noise to the observed spectra, we attempted to quantify the contribution of electronic noise to the observed spectra.

The electronic noise spectra for the microstructure sensors were determined in a laboratory setting by replacing the micro-conductivity and temperature cells with resistors and the shear probes with capacitors and then recording the output of the microsctructure electronics modules with the HRP computer. Vaules of resistance were chosen to return steady state outputs corresponding to 3° C and 40 mmho/cm for the micro-temperature and conductivity sensors. The shear probes (1500 pF nominal capacitance) were replaced with 1000 pF mica capacitors. The electronic noise spectra for the temperature and conductivity sensors reveal an approximate ω^2 dependence while the electronic noise spectra for the shear probes are approximately white, Figure 3. After scaling the electronic noise spectra and applying transfer functions appropriate for the oceanic data displayed in Figure 2, the electronic noise spectra are approximately equal to the minimum observed spectral densities at frequencies greater than 10 Hz for both the temperature and conductivity sensors, Figure 2. Electronic noise thus provides the noise floor for the temperature and conductivity sensors. A similar analysis of the electronic noise spectra for the shear probes suggests that electronic noise provides the noise floor at frequencies smaller than 5 Hz for the shear probes, Figure 2. The electronic noise for the shear probe electronics is associated with 1/f noise in the input amplifier, which is then differentiated and appears as white noise (R. Koehler, personal communication, 1996). The uncertainty in the dissipation rate resulting from electronic noise, obtained by integrating the scaled electronic noise spectra over the minimum bandwidth $0.78 - 4.7$ Hz, is $4x10^{-12}$ W/kg. Slight modifications to the shear probe electronics were made after the NATRE cruise. We infer an uncertainty associated with electronic noise of approximately $8x10^{-12}$ W/kg for the data appearing in Figure 2. The Johnson noise associated with the shear probe is potentially large (the nominal probe resistance is approximately $2x10^{11}$ohm!) but does not appear in the observed spectra: the probe resistance is mismatched with the effective load resistance of the input amplifier, thereby reducing the Johnson noise across the input amplifier.

The dissipation estimates are also subject to noise resulting from a variety of mechanical sources. Both the peak at high frequencies (30–40 Hz) and the smaller peak at 10 Hz in the observed shear spectra are thought to result from vibration. Turbulent wake formation from the CTD head is believed to be the primary source of vibrational energy. The microstructure temperature sensor consists of a thermistor encased in a thin, drawn glass coating. The glass coating is not uniform and these irregularities are subject to cracking under pressure, which increase the noise level of the sensor. Increased noise levels are typically noted for temperature sensors with time constants determined from a regression against the conductivity cell (Section IV) smaller than the nominal value of 7 ms, consistent with thinner glass coatings being more sensitive to cracking induced noise.

The noise levels of the HRP are sufficiently small as to allow the resolution of weak mixing ($K \sim 0.1x10^{-4}$ m^2 s^{-1}) in regions of weak abyssal stratification ($N^2 = 5x10^{-7}$ s^{-2}, $\theta_z = 5x10^{-4}$ °C m^{-1}, implying dissipation rates of $\epsilon = 2x10^{-11}$ Wkg^{-1} and $\chi_\theta = 5x10^{-12}$ $°C^2$ s^{-1}). Recent measurements (Toole *et al.*, 1994; Polzin *et al.*, submitted) suggest that the abyssal interior above smooth bottom topography supports only weak mixing which contributes little to spatially averaged turbulent heat and mass fluxes. The implication is that the bulk of the turbulent fluxes occur in hot spots (Polzin *et al.*, 1996) or above rough bathymetry (Polzin *et al.*, submitted). With noise levels of $\epsilon \cong 10^{-10}$ Wkg^{-1}, the contribution of regions above smooth topography to the spatially averaged turbulent fluxes would be uncertain and the importance of 'hot spots' and rough bathymetry much less apparent. While the study of weak mixing is not intrinsically as interesting as the study of mixing in 'hot spots' or above rough bathymetry, defining the small background levels of turbulent mixing is nevertheless an important result. The low microstructure noise levels of the HRP permit an accurate assessment of the spatial variability of turbulent mixing in the abyssal ocean.

The dissipation noise levels are sufficiently small as to raise fundamental questions about the interpretation of dissipation estimates in a stratified fluid. At weak levels of turbulent intensity, buoyancy forces dominate inertial (nonlinear) forces at all vertical scales and suppress overturning (Itsweire *et al.*, 1993). Laboratory data and numerical simulations both reveal a zero net buoyancy flux at dissipation rates smaller

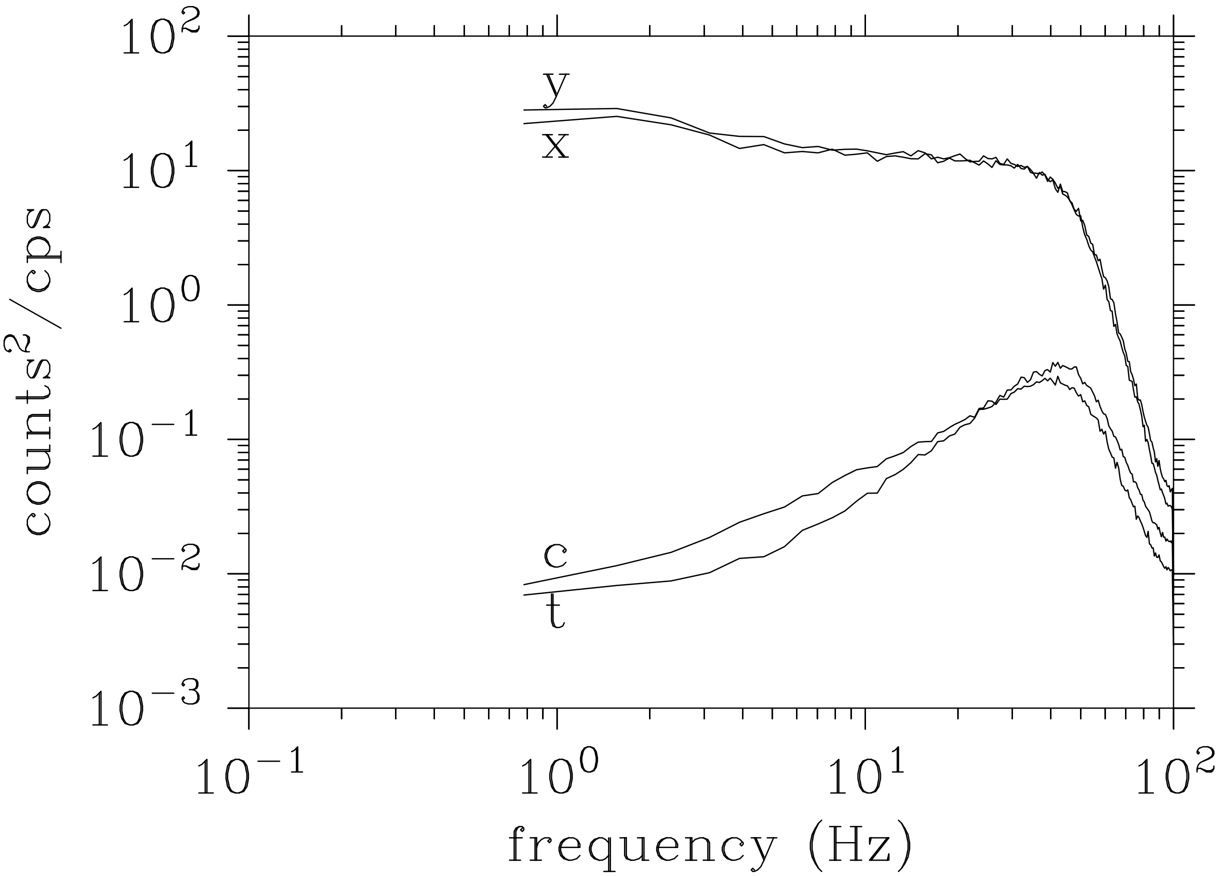

Figure 3: Laboratory determined electronic noise spectra for shear (x and y), microtemperature (t) and microconductivity (c) channels, as recorded by the HRP. The decreasing trend of sepctral density for frequencies greater than 50 Hz is associated with anti-aliasing filters. The ordinate has units of digitizer counts squared per cycle per second.

than $\epsilon < 16\nu N^2$ (Rohr *et al.*, 1988; Itsweire *et al.*, 1993). Thus it may be inappropriate to interpret dissipations smaller than $16\nu N^2$ in terms of a gradient diffusion process (1). For the data in Figure 2, $\nu = 1.5x10^{-6}$ m^2 s^{-1} and $N^2 = 1.1x10^{-6}$ s^{-2}, so that $16\nu N^2 = 3x10^{-11}$ W/kg, higher than the electronic noise level. Questions about the use of isotropy also arise for small values of $\epsilon/\nu N^2$ (e.g. Gargett *et al.*, 1984; Itsweire *et al.*, 1993). We believe that the fundamental uncertainty in the dissipation estimates is not the uncertainty in the estimates of shear variance associated with noise being interpreted as turbulence, rather it is in the interpretation of shear variance in the framework of stratified turbulence.

7 Summary

The HRP, designed and developed at the Woods Hole Oceanographic Institution, provides high quality data over vertical scales of 1000 to 1 cm. The instrumentation and sensors of the HRP, combined with rigorous software processing, has made possible our studies of turbulent mixing in the deep ocean, an important and poorly understood link in the thermohaline circulation of the World's ocean. The attainment of low-noise microstructure variance estimates is crucial to this endeavor.

8 ACKNOWLEDGMENTS

The HRP group gratefully acknowledges the continuing unselfish advice and assistance of Neil Oakey. He provided his software upon which the HRP microstructure processing routines are based, the design for the shear probe electronics, and has made available resources for shear probe calibration.

9 REFERENCES

Dugan, J. P., and B. W. Stalcup, Comparison of towed conductivity sensor performance, *JOAT*, **5**, 116-122, 1988:

Gargett, A. E., T. R. Osborn and P. W. Nasmyth, 1984: Local isotropy and the decay of turbulence in a stratified fluid. *Journal of Fluid Mechanics*, **144**, 231–280.

Gregg, M. C., T. Meagher, A. Pederson and E. Aagaard, 1978: Low noise temperature microstructure measurements with thermistors, *Deep-Sea Research*, **25**, 843–856.

Gregg, M. C. and T. Meagher, 1980: The dynamics response of glass road thermistors, *Journal of Geophysical Research*, **85**, 2779–2786.

Gregg, M. C., E. A. D'Asaro, T. J. Shay and N. Larson, 1986: Observations of persistent mixing and near-inertial internal waves, *Journal of Physical Oceanography*, **16**, 856–885.

Gregg, M. C., H. E. Seim and D. B. Percival, 1993: Statistics of shear and turbulent dissipation profiles in random internal wave fields. *Journal of Physical Oceanography*, **23**, 1777–1799.

Head, M. J., 1983: The use of miniature four-electrode conducitivity probes for high resolution measurement of turbulent density or temperature variations in salt-stratified water flows, Ph.D. dissertation, University of California at San Diego, 211 pp.

Holt, S. E., J. R. Koseff and J. H. Ferziger, 1992: A numerical study of the evolution and structure of homogeneous stably stratified sheared turbulence. *Journal of Fluid Mechanics*, **237**, 499–540.

Itsweire, E. C., J. R. Koseff, D. A. Briggs and J. H. Ferziger, 1993: Turbulence in stratified shear flows: Implications for interpreting shear-induced mixing in the ocean. *Journal of Physical Oceanography*, **23**, 1508–1522.

Lueck, R. G., O. Hertzman and T. R. Osborn, 1977: The spectral response of thermistors, *Deep-Sea Research*, **24**, 951-970.

Lueck, R. G. and T. R. Osborn, 1980: The characteristics of internally heated thermistors, *Deep-Sea Research*, **27**, 273–292.

Meagher, T., A. Pedersen and M. Gregg, 1982: A low noise conductivity microstructure instrument, Proc. of IEEE Oceans ′82, 282–290.

Marmarino, G. O., J. P. Dugan and T. E. Evans, 1986: Horizontal variability of microstructure in the vicinity of a Sargasso Sea Front, *Journal of Physical Oceanography*, **16**, 967–980.

Mellinger, E. C., K. E. Prada, R. L. Koehler and K. W. Doherty, 1986: Instrument Bus: An electronic system architecture for oceanographic instrumentation. Woods Hole Oceanographic Institution Technical Report, WHOI-86-30, 86 pp.

Montgomery, E. T. and J. M. Toole, 1993: Fine– and Microstructure Observations at Fieberling Guyot *RV New Horizon* Cruise Report. WHOI Technical Report, WHOI -93-51 27 pp.

Montgomery, E. T. and R. W. Schmitt, 1993: Cruise Report – *Oceanus* 250 Leg 4 High Resolution Profiler Survey for the North Atlantic Tracer Release Experiment: (NATRE) March 25–April 24, 1992. WHOI Technical Report, WHOI-93-39, 41 pp.

Montgomery, E. T., 1996: Cruise Report – High Resolution Profiler Study of Deep Mixing in the Romanche Fracture Zone. WHOI Technical Report, WHOI-96-12, 23pp.

Montgomery, E. T., 1996: Cruise Report – High Resolution Profiler Survey for the Brazil Basin Tracer Release Experiment and (BBTRE): *RV/Seward Johnson*, January–February, 1996. unpublished

Ninnis, R., 1984: The effects of spatial averaging on airfoil probe measurements of oceanic velocity microstructure, Ph.D. dissertation, 109 pp., University of British Columbia, Vancouver.

Oakey, N. S., 1977: An instrument to measure oceanic turbulence and microstructure, Bedford Inst. Oceanogr. Rep. Ser. BI-R-77-3, **52** pp.

Oakey, N. S., 1982: Determination of the rate of dissipation of turbulent energy from simultaneous temperature and velocity microstructure measurements, *Journal of Physical Oceanography*, **12**, 256–271.

Okawa, B. S., and J. P. Dugan, 1984: Contamination of conductivity measurements by waterborn particles. Ocean Eng., **11**, 265–279.

Osborn, T. R., C. S. Cox, 1972: Oceanic fine structure, *Geophysical Fluid Dynamics*, **3**, 321–345.

Osborn, T. R., 1974: Vertical profiling of velocity microstructure, *Journal of Physical Oceanography*, **4**, 109-115.

Osborn, T. R., 1980: Estimates of the local rate of vertical diffusion from dissipation measurements, *Journal of Physical Oceanography*, **10**, 83–89.

Osborn, T. R. and W. R. Crawford, 1980: An airfoil probe for measuring turbulent velocity fluctuations in water, *Air-Sea Interactions: Instruments and Methods*, F. Dobson, L. Hasse and R. Davis, Eds., Plenum Press, 801 pp.

Polzin, K. L., K. G. Speer, J. M. Toole and R. W. Schmitt, 1996: Intense mixing of Antarctic Bottom Water in the equatorial ocean. *Nature*, **380**, 54–57.

Polzin, K. L., J. M. Toole, J. R. Ledwell and R. W. Schmitt, 1996: Spatial variability of turbulent mixing in the abyssal ocean. Submitted to *Science*.

Rohr, J. J., K. N. Helland, E. C. Itsweire, and C. W. Van Atta, 1988: Growth and decay of turbulence in a stably stratified shear flow. *Journal of Fluid Mechanics*, **195**, 77–111.

Schmitt, R. W., J. M. Toole, R. L. Koehler, E. C. Mellinger, and K. W. Doherty, 1988: The development of a fine- and microstructure profiler. *Journal of Atmospheric and Oceanic Technology*, **5**(4), 484–500.

Schmitt, R. W. and E. T. Montgomery, 1991: Cruise Report, OCEANUS 218. Warm ring inertial critical layer experiment (WRINCLE). WHOI Tech Rpt. 91–33.

Stern, M. E., 1975: Ocean circulation physics, Academic Press New York, 246 pp.

Toole, J. M., K. L. Polzin and R. W. Schmitt, 1994: Estimates of diapycnal mixing in the abyssal ocean. *Science*, **264**, 1120–1123.